NACA

RESEARCH MEMORANDUM

EFFECT OF WING FLEXIBILITY ON THE DAMPING IN ROLL OF A NOTCHED DELTA WING-BODY COMBINATION BETWEEN MACH NUMBERS 0.6 AND APPROXIMATELY 2.2 AS DETERMINED WITH ROCKET-PROPELLED MODELS

By William M. Bland, Jr.

Langley Aeronautical Laboratory
Langley Field, Va.

NATIONAL ADVISORY COMMITTEE
FOR AERONAUTICS

WASHINGTON
June 18, 1954

NATIONAL ADVISORY COMMITTEE FOR AERONAUTICS

RESEARCH MEMORANDUM

EFFECT OF WING FLEXIBILITY ON THE DAMPING IN ROLL OF A NOTCHED DELTA WING-BODY COMBINATION BETWEEN MACH NUMBERS 0.6 AND APPROXIMATELY 2.2 AS DETERMINED WITH ROCKET-PROPELLED MODELS

By William M. Bland, Jr.

SUMMARY

An experimental investigation employing sting-mounted rocket-propelled models in free flight at approximately zero lift has been made to determine the effect of wing flexibility on the damping-in-roll characteristics of a wing-body combination in the range of Mach numbers from 0.6 to approximately 2.2. The wing used in this investigation had a notched delta plan form of aspect ratio 3.2 with leading edges swept back 55°, trailing edges swept back 10°, and NACA 65A003 airfoil sections parallel with the model center line. The results of this investigation indicated that increasing wing flexibility by changing from a solid-steel wing to a solid-magnesium wing decreased the damping in roll as much as 32 percent except in the range of Mach numbers from 1.0 to 1.4 where the decrease was generally less than 8 percent. Also, it was shown that the damping in roll estimated for a rigid wing from the experimental results agreed very well with values predicted by theory in the supersonic region, and was higher in the subsonic region than values obtained from empirical data.

INTRODUCTION

Accurate knowledge of the lateral stability derivatives is essential for evaluation of the dynamic lateral stability characteristics of airplane and missile configurations. In general, the theoretical methods for determining the lateral stability derivatives, many of which are summarized in reference 1, are based upon the hypothesis of rigid wings. Likewise, much of the experimental work, summarized in reference 2, has been done under conditions that either approach the rigid-wing condition or do not take wing flexibility into account whatsoever. The continuing

trend combining higher flight speeds with corresponding higher loads and thinner wings, which have less resistance to bending and twisting, makes it necessary to modify the rigid-wing values of some of the stability derivatives in order to account for distortion of wing structure under aerodynamic loads.

In order to determine the effect of wing flexibility on the damping-in-roll derivative, the Langley Pilotless Aircraft Research Division has conducted an investigation using a notched delta wing-body configuration. The notched delta wing had an aspect ratio of 3.2 with leading edges swept back 55°, trailing edges swept back 10°, and NACA 65A003 airfoil sections parallel with the body center line. In this investigation, which was conducted with a testing technique utilizing sting-mounted rocket-propelled models in free-flight, two models were tested. One had a solid-steel wing and the other had a much more flexible wing made of solid magnesium. Results of this investigation were obtained in the range of Mach numbers from 0.6 to approximately 2.2, corresponding to a range of Reynolds numbers from approximately 0.7×10^6 to 5.0×10^6 (based on wing mean aerodynamic chord). The flight tests were conducted at the Langley Pilotless Aircraft Research Station at Wallops Island, Va.

SYMBOLS

b	wing span, ft
b'	wing span, in.
S	total included wing area, sq ft
c	chord, ft
$\bar{c}$	mean aerodynamic chord, ft
c_{av}	average chord S/b, ft
λ	taper ratio
$\Lambda_{c/4}$	sweepback of quarter-chord line, deg
y	distance from model center line to any point on wing, perpendicular to center line, in.
A	aspect ratio
i	incidence, deg

[redacted]

θ	angular deflection per unit length, in plane parallel with plane of symmetry, radians
m	moment in plane parallel with plane of symmetry, in-lb
G	shear modulus of elasticity, lb/sq in.
J	torsional stiffness constant of airfoil cross section in plane parallel to plane of symmetry, $in.^4$
q	dynamic pressure, lb/sq ft
V	velocity, ft/sec
p	rolling velocity, radians/sec
M	Mach number
R	Reynolds number, based on $\bar{c}$
L	rolling moment, ft-lb
$\frac{pb}{2V}$	wing-tip helix angle, radians
C_l	rolling-moment coefficient, L/qSb
C_{l_p}	damping-in-roll derivative per radian, $\frac{dC_l}{d\frac{pb}{2V}}$
c_l	local lift coefficient, $\frac{\text{Local lift}}{qS}$
C_L	wing lift coefficient, $\frac{\text{Total lift}}{qS}$
C_{L_α}	lift-curve slope per degree
$\frac{c_l c}{C_L c_{av}}$	spanwise loading coefficient

[redacted]

Subscripts:

m	measured
a	adjusted
ma	misalinement
r	rigid
f	flexible

MODELS

The wing-body configuration used in this investigation is shown in figure 1. The wing had a notched delta plan form of aspect ratio 3.2, leading-edge sweepback of 55°, trailing-edge sweepback of 10°, and NACA 65A003 airfoil sections parallel with the body center line. Two models of this configuration were tested: one with a one-piece solid-steel wing and the other with a one-piece solid-magnesium wing. The wing of each model was clamped in a midwing position to identical, pointed, cylindrical steel bodies. The wing dimensions shown in figure 1 are nominal. Actual measurements to the physical wing tips gave the following results:

	b	S	Wing-tip radius, in.
Steel wing	0.810	0.215	0.140
Magnesium wing	.802	.213	.188

These values were used in the computation of the rolling-moment coefficient and the wing-tip helix angle.

The dull appearance of the model in figure 2 was caused by a protective plastic coating which was removed before flight. Actually, the wing and body surfaces were carefully machined and polished.

Preflight measurements of the models disclosed that the wings had misalinements relative to the model center line which were caused by construction inaccuracies. Results of these measurements are presented in figure 3.

[redacted]

TEST PROCEDURE

Each model tested during this investigation was attached to the sting-like forward section of a carrier vehicle as shown in figures 2 and 4. This sting-like section contained a torsion balance for measuring the rolling moment generated by the model as it was forced to roll by the carrier vehicle which had twisted stabilizing fins. During flight, time histories of the rolling moment, rolling velocity, and flight-path velocity were obtained by telemeter, radio, and radar. These measurements were used in conjunction with radiosonde measurements of atmospheric conditions encountered to permit evaluation of the damping-in-roll derivative as a function of Mach number. A description of this testing technique is given in reference 3. In the present tests a booster rocket-motor assembly (fig. 4), which separated from the model—carrier-vehicle combination as soon as its fuel was exhausted, was used to extend the Mach number range of the investigation.

DATA

Data Reduction and Adjustment

The rolling-moment and rolling-velocity data obtained for each model were converted to rolling-moment coefficients and wing-tip helix angles as functions of Mach number. By assuming linearity of C_l with $pb/2V$, C_{l_p} was obtained from the relation

$$C_{l_p} = \frac{C_l}{pb/2V}$$

However, the values of C_{l_p} determined thusly and presented in figure 5 as functions of Mach number have not been adjusted to compensate for the measured wing misalinements due to construction inaccuracies.

An equation for the rolling-moment coefficient due to wing misalinement

$$C_{l_{ma}} = \frac{C_{L_\alpha}}{(b')^2}\int_{b'/2}^{b'/2} \frac{c_l c}{C_L c_{av}}\, i_y\, dy$$

has been derived by using strip theory. Evaluating this equation for each of the models used in this investigation by using the spanwise

incidence variation presented in figure 3 and an elliptical variation of the spanwise loading coefficient throughout the Mach number range resulted in the following expressions:

$$\left(C_{l_{ma}}\right)_f = 0.04203\left(C_{l_\alpha}\right)_f \quad \text{(steel-wing model)}$$

$$\left(C_{l_{ma}}\right)_f = 0.04753\left(C_{l_\alpha}\right)_f \quad \text{(magnesium-wing model)}$$

Where $\left(C_{l_\alpha}\right)_f$ is the apparent lift-curve slope (per degree) of the particular flexible wing.

The torsional stiffness of a wing can be expressed in terms of angular deflection per unit moment

$$\frac{\theta}{m} = \frac{1}{GJ}$$

Comparative stiffness of wings that are geometrically identical (condition of equal torsional stiffness constants) can be expressed in terms of the inverse ratio of the respective shear moduli. From this condition, the values of $\left(C_{l_p}\right)_r$ were obtained by linear extrapolation of $\left(C_{l_p}\right)_m$ values at the same Mach numbers to a value of $1/G = 0$. Values of $\left(C_{l_\alpha}\right)_f$ for evaluating the expressions for $\left(C_l\right)_{ma}$ were then obtained by the approximation

$$\left(C_{l_\alpha}\right)_f = \left(C_{l_\alpha}\right)_r \frac{\left(C_{l_p}\right)_m}{\left(C_{l_p}\right)_r}$$

This approximation was used because it was believed to be the best one available; however, it should be remembered that the outboard regions of a wing contribute the largest portion of C_{l_p} and that it is these same regions of a delta wing with a constant thickness ratio that distort the most under load (ref. 4). Thus, changes in C_{l_p} may not always be proportional to changes in C_{l_α}.

The variation of $\left(C_{l_\alpha}\right)_r$ with Mach number as obtained from various sources is presented in figure 6. The $\left(C_{l_\alpha}\right)_r$ values for $M > 1.4$ were

obtained for a wing-body combination in reference 5. Values between $M = 0.6$ and $M = 0.9$ were obtained by applying suitable compressibility modifications from reference 6 to lift-curve-slope values obtained from unpublished data for a similar wing-body combination. The curve between $M = 0.9$ and $M = 1.4$ was obtained by fairing through theoretical wing-alone values from reference 7 and experimental values presented in reference 8 for a 52.5° sweptback delta wing-body combination in such a manner that the end points faired smoothly into the values for $M \leqq 0.9$ and $M \geqq 1.4$.

With the assumption that changes in the rolling moment generated by the model would not affect $\left(\frac{pb}{2V}\right)_m$ of the model—carrier-vehicle combination and since the wing misalinements for both models were distributed so as to generate a rolling moment opposite in direction to the rolling moment due to roll, the expression for the adjusted damping-in-roll derivative becomes

$$\left(C_{l_p}\right)_a = \left(C_{l_p}\right)_m + \frac{C_{l_{ma}}}{(pb/2V)_m}$$

The percentage differences between measured and adjusted C_{l_p} values, based on the adjusted values, are as follows:

M	Steel wing	Magnesium wing
0.8	29	36
1.0	39	42
1.5	28	31
2.0	29	32

The adjusted values of C_{l_p} can be expected to be somewhat high, depending on how much the actual variation of the spanwise loading coefficient differs from the assumed elliptical variation.

Accuracy

Experience with this technique has shown that the maximum possible systematic errors in the measured quantities due to inherent limitations in the measuring, recording, and data reduction systems are within the following limits:

M	$(\Delta C_{l_p})_m$
0.8	±0.028
1.0	±.017
1.5	±.005
2.0	±.003

The maximum possible error in Mach number is believed to be within ±0.01 throughout the Mach number range.

RESULTS AND DISCUSSION

The measured values of the damping-in-roll derivative, presented in figure 5, were obtained at approximately zero lift and at a nearly constant wing-tip helix angle of 0.03 radian throughout the Mach number range of the investigation. The variations of the wing-tip helix angle and the Reynolds number, based on $\bar{c}$, with Mach number are presented in figure 7. Adjusting the measured C_{l_p} values for construction inaccuracies as described in the data section resulted in the variations of the damping-in-roll derivative with Mach number presented in figure 8 for the two models tested.

These results show that changing the wing material from steel to magnesium resulted in large reductions in the damping-in-roll derivative at high subsonic Mach numbers (about 26 percent at $M = 0.6$ and 32 percent at $M = 0.8$) and at the higher Mach numbers of the test (about 22 percent at $M = 1.6$ and over 31 percent at $M = 2.2$). At the intermediate Mach numbers, between $M = 1.0$ and $M = 1.4$, the results indicated less reduction in the damping-in-roll derivative, generally less than 8 percent of the value obtained for the model with the steel wing. Even though the loads resulting from the wing misalinements were large compared with the loads due to forced roll, a comparison of the reductions in C_{l_p} due to wing flexibility in figure 5 (before misalinement adjustments) with those in figure 8 (after misalinement adjustments), which generally agree within 4 percent, indicates that essentially the reductions in C_{l_p} shown in figure 8 and previously discussed apply to the wing without initial misalinement.

Also included in figure 8 is an estimated curve representing the variation of C_{l_p} with Mach number for a rigid wing. This curve was obtained by plotting the adjusted C_{l_p} values obtained for the models

with the steel and the magnesium wings against the inverse of the appropriate shear modulus, $\frac{1}{G} = \frac{1}{12000000}$ for the steel wing and $\frac{1}{G} = \frac{1}{2400000}$ for the magnesium wing, and by extrapolating linearly to $\frac{1}{G} = 0$.

The estimated C_{l_p} curve for the rigid wing is compared in figure 9 with reference material. Between $M = 1.4$ and the upper Mach number limit of the present investigation the damping in roll estimated for a rigid wing agrees very well with that calculated by existing supersonic theories in reference 5 for a wing-body combination with a geometrically similar wing. Good agreement was also obtained throughout the comparable Mach number range with damping-in-roll values calculated by the method of reference 9 which is based upon linearized potential flow.

At subsonic speeds, the damping in roll estimated for the rigid wing and experimentally determined for the steel wing are considerably higher than the damping in roll obtained by applying the compressibility corrections of reference 6 to empirical data of reference 10. A similar comparison was noted in reference 3 for damping-in-roll values obtained for a solid-steel, 4-percent-thick, aspect-ratio-4, delta wing.

CONCLUSIONS

The results of an investigation made with a technique employing sting-mounted rocket-propelled models to determine the effect of wing flexibility on the damping-in-roll derivative at approximately zero lift of a wing-body combination with a notched delta wing of aspect ratio 3.2 in the range of Mach numbers from 0.6 to approximately 2.2 indicate the following conclusions:

1. Making the wing much more flexible by changing the wing material from solid steel to solid magnesium decreased the value of the damping-in-roll derivative as much as 32 percent in the subsonic region and as much as 30 percent in the high supersonic range of the investigation; between Mach numbers 1.0 and 1.4 the decrease was generally less than 8 percent.

2. The damping in roll estimated for a rigid wing from the experimental results agreed very well with values predicted by theory in the

supersonic region, and was higher than values derived from empirical data in the subsonic region.

Langley Aeronautical Laboratory,
National Advisory Committee for Aeronautics,
Langley Field, Va., April 28, 1954.

REFERENCES

1. Jones, Arthur L., and Alksne, Alberta: A Summary of Lateral-Stability Derivatives Calculated for Wing Plan Forms in Supersonic Flow. NACA Rep. 1052, 1951.

2. Malvestuto, Frank S., Jr., and Kuhn, Richard E.: Examination of Recent Lateral-Stability-Derivative Data. NACA RM L53I08a, 1953.

3. Bland, William M., Jr., and Sandahl, Carl A.: A Technique Utilizing Rocket-Propelled Test Vehicles for the Measurement of the Damping in Roll of Sting-Mounted Models and Some Initial Results for Delta and Unswept Tapered Wings. NACA RM L50D24, 1950.

4. Stein, Manuel, Anderson, J. Edward, and Hedgepeth, John M.: Deflection and Stress Analysis of Thin Solid Wings of Arbitrary Plan Form With Particular Reference to Delta Wings. NACA Rep. 1131, 1953. (Supersedes NACA TN 2621.)

5. Margolis, Kenneth, and Bobbitt, Percy J.: Theoretical Calculations of the Stability Derivatives at Supersonic Speeds for a High-Speed Airplane Configuration. NACA RM L53G17, 1953.

6. Fisher, Lewis R.: Approximate Corrections for the Effects of Compressibility on the Subsonic Stability Derivatives of Swept Wings. NACA TN 1854, 1949.

7. Piland, Robert O.: Summary of the Theoretical Lift, Damping-in-Roll, and Center-of-Pressure Characteristics of Various Wing Plan Forms at Supersonic Speeds. NACA TN 1977, 1949.

8. Kehlet, Alan B.: Aerodynamic Characteristics at Transonic and Supersonic Speeds of a Rocket-Propelled Airplane Configuration Having a 52.5° Delta Wing and a Low, Swept Horizontal Tail. NACA RM L54A20, 1954.

9. Malvestuto, Frank S., Jr., and Margolis, Kenneth: Theoretical Stability Derivatives of Thin Sweptback Wings Tapered to a Point With Sweptback or Sweptforward Trailing Edges for a Limited Range of Supersonic Speeds. NACA Rep. 971, 1950. (Supersedes NACA TN 1761.)

10. Goodman, Alex, and Adair, Glenn H.: Estimation of the Damping in Roll of Wings Through the Normal Flight Range of Lift Coefficient. NACA TN 1924, 1949.

[redacted]

[redacted]

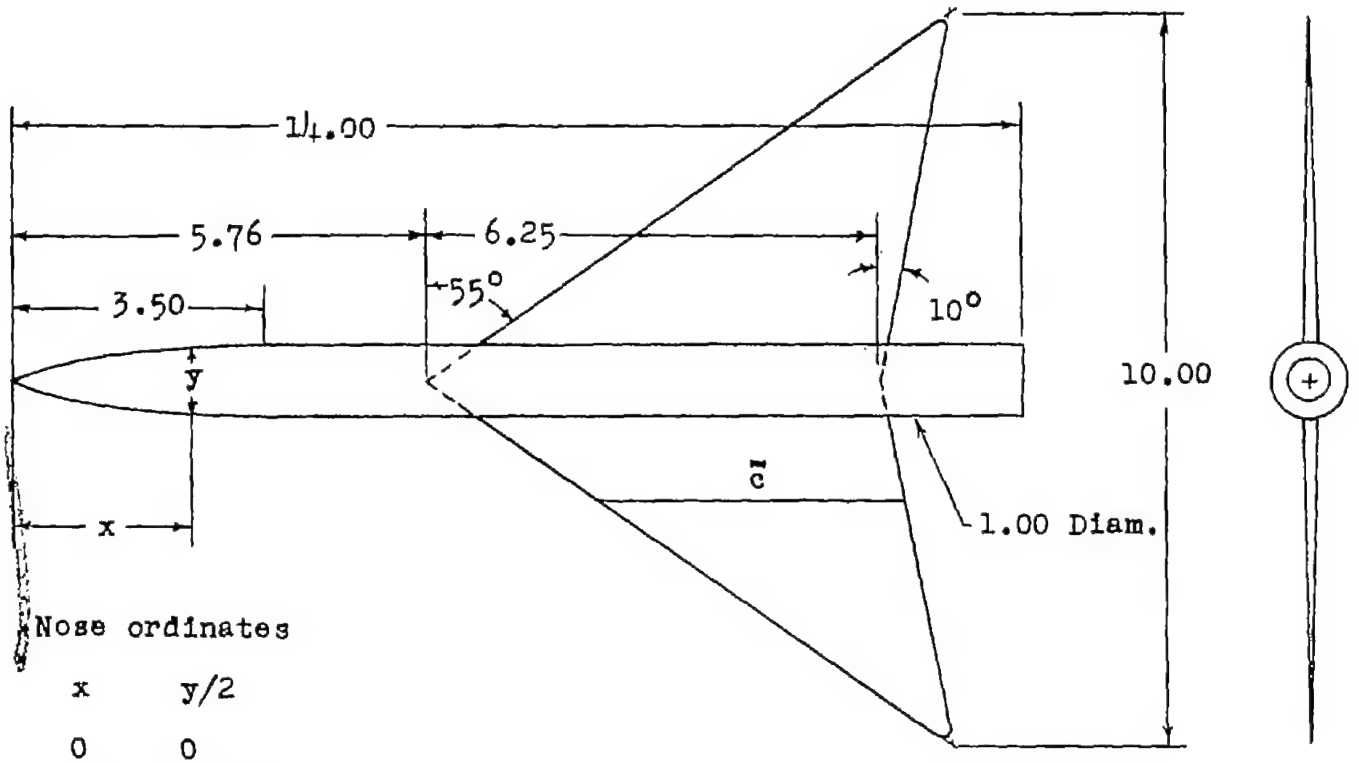

Nose ordinates

x	y/2
0	0
0.2	0.050
.4	.096
.6	.142
1.0	.226
1.5	.314
2.0	.391
2.5	.450
3.0	.486
3.5	.500

Wing details

S	0.217 sq ft
A	3.2
$\bar{c}$	0.346 ft
λ	0
$\Lambda_{c/4}$	48.2°
Airfoil	NACA 65A003

Figure 1.- Sketch and details of configuration tested. All dimensions are in inches except where noted.

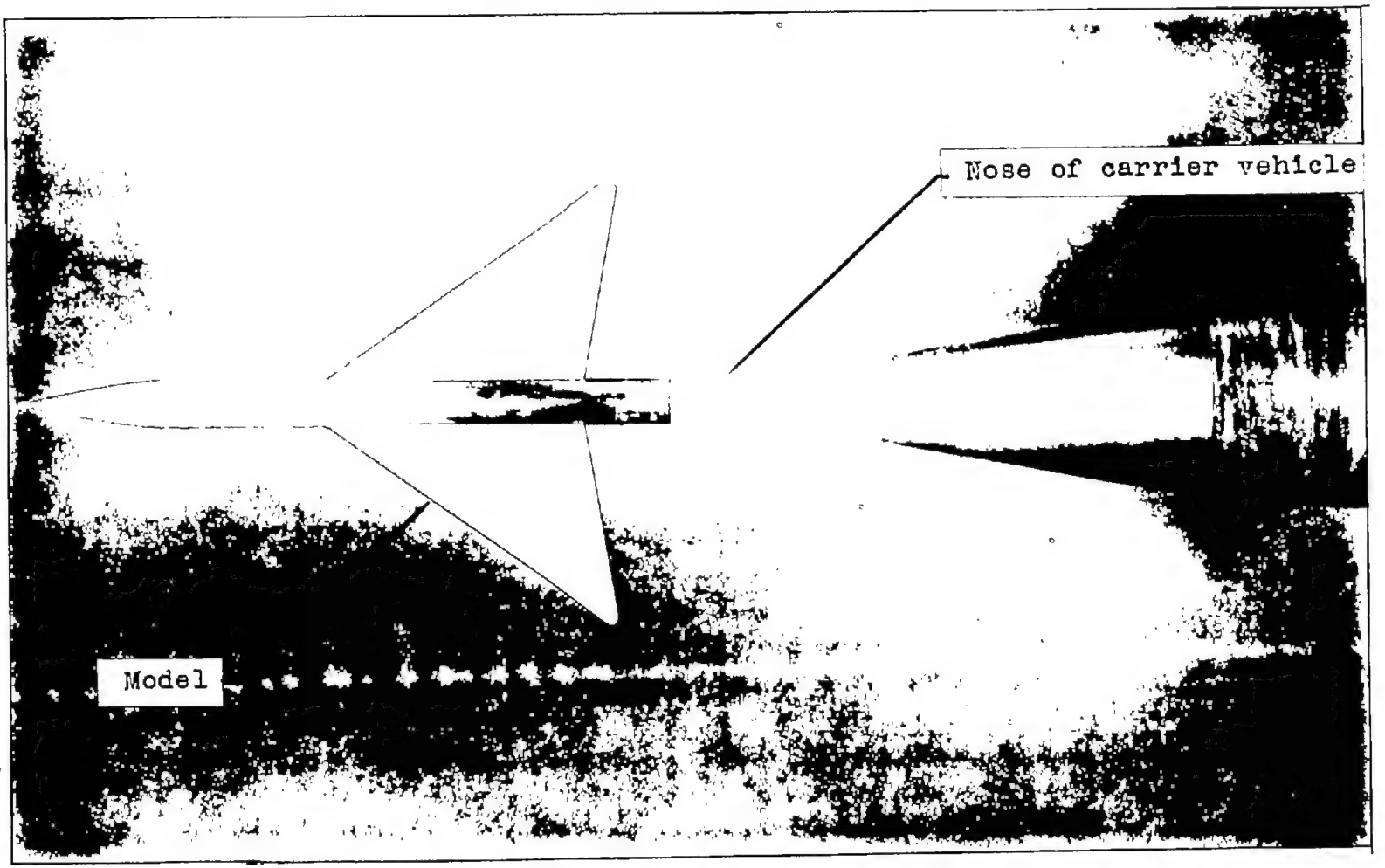

L-80698.1

Figure 2.- Model mounted on nose of carrier vehicle.

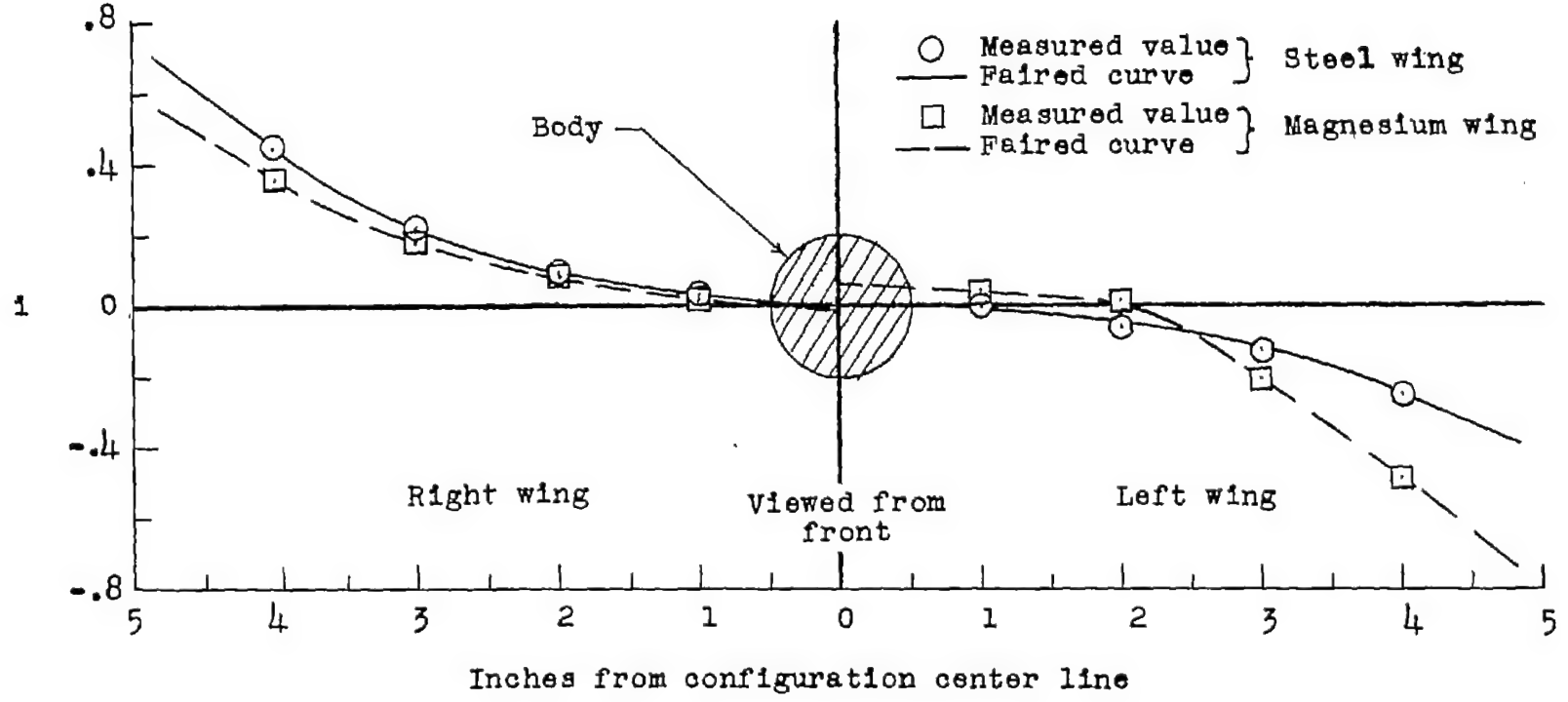

Figure 3.- Variation of incidence along wing span. Positive incidence on right wing and negative incidence on left wing give rolling moment opposite to rolling moment due to rolling velocity.

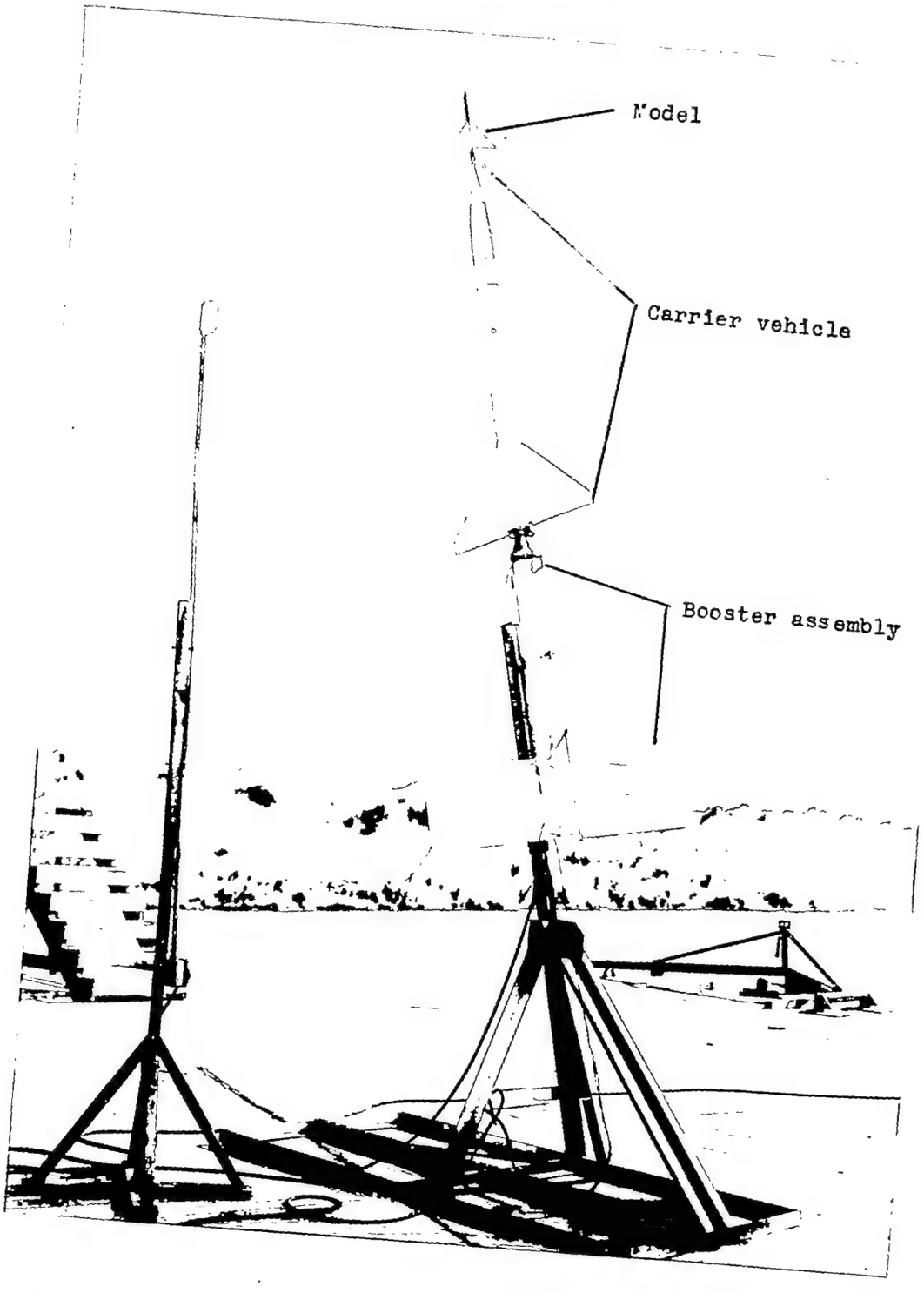

Figure 4.- Model, carrier vehicle, and booster rocket-motor assembly on launcher. L-81906.1

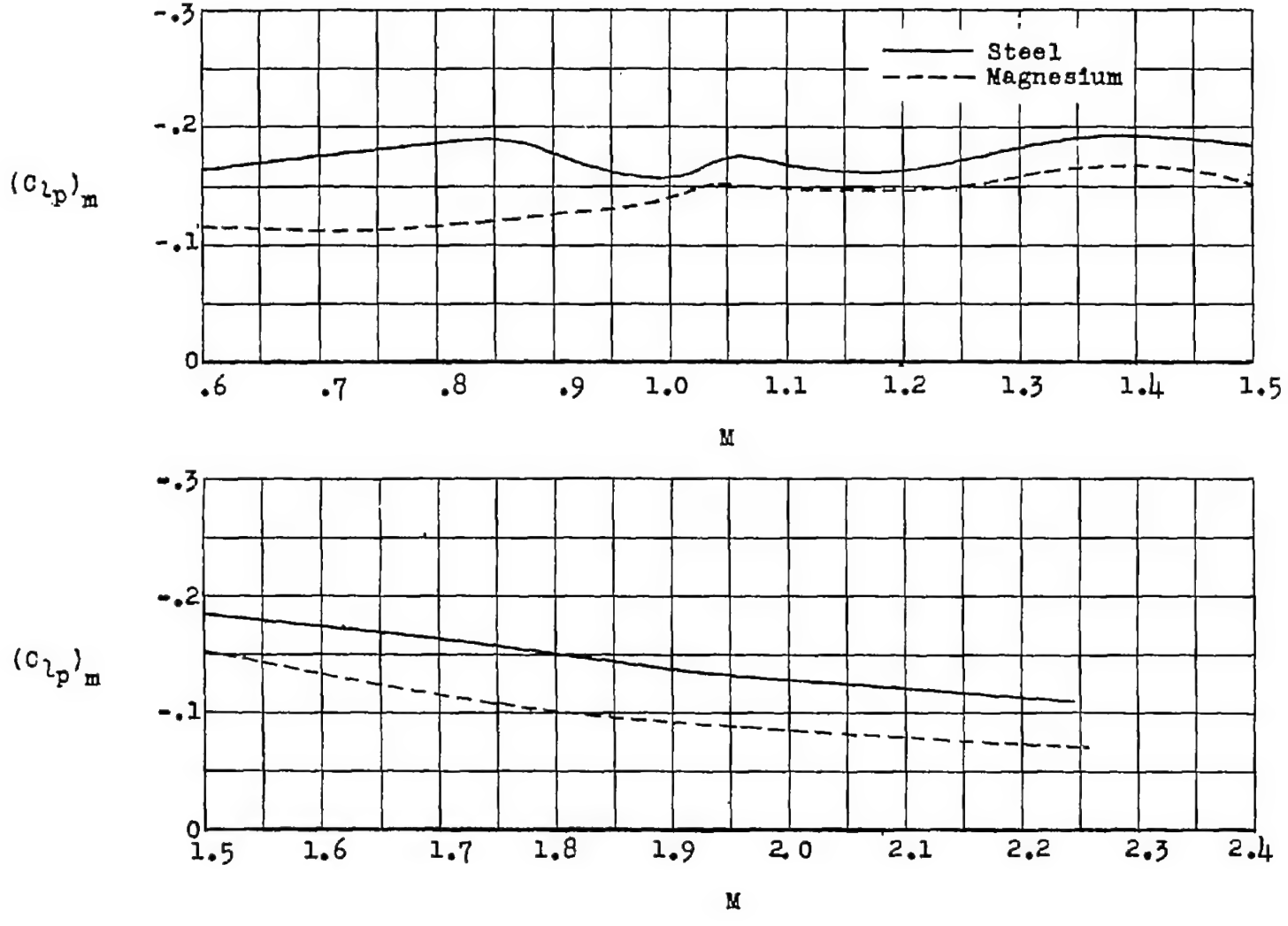

Figure 5.- Variation with Mach number of damping-in-roll derivative without adjustment for wing misalinement.

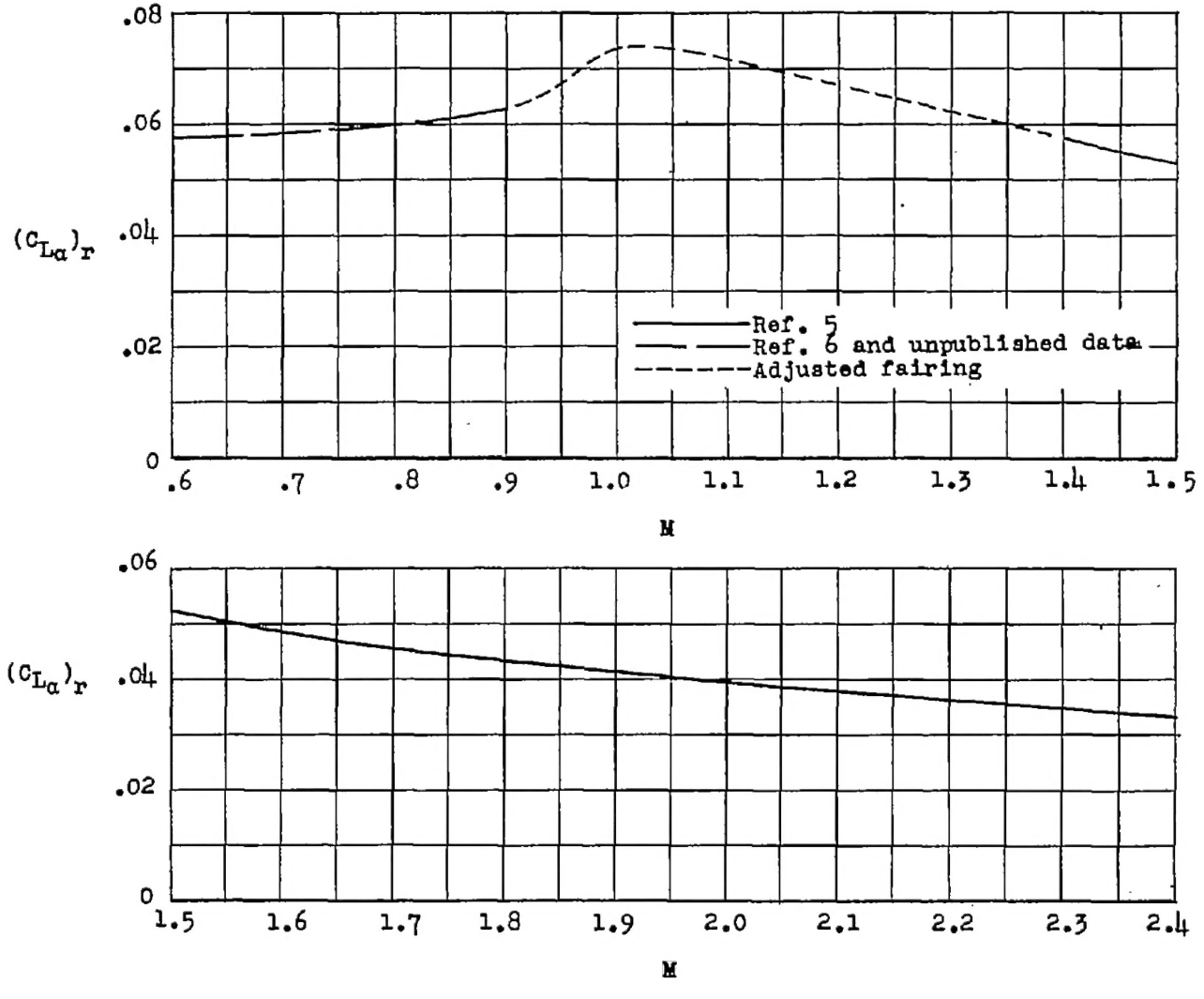

Figure 6.- Variation of lift-curve slope with Mach number used to adjust measured damping-in-roll values for wing misalinements.

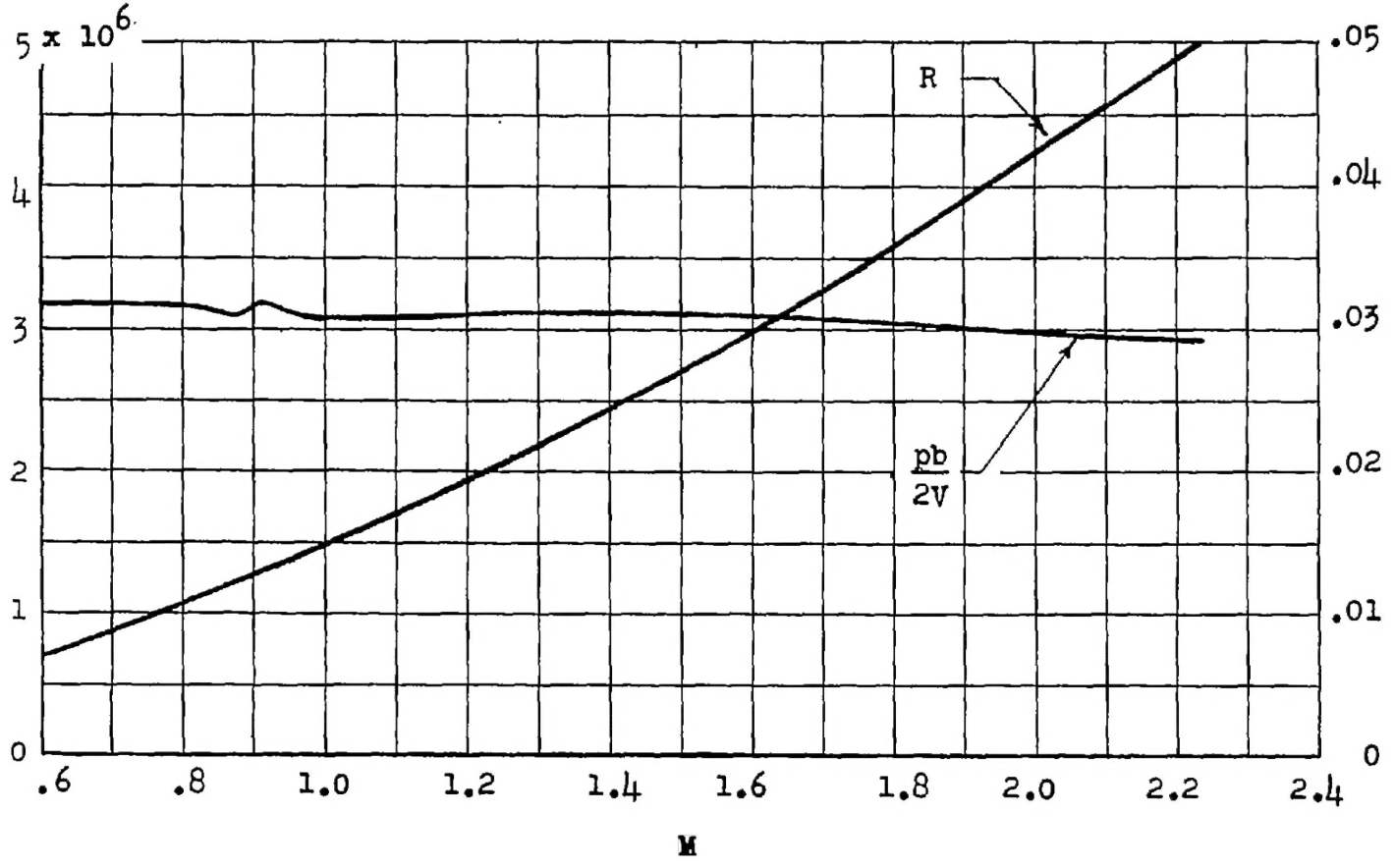

Figure 7.- Variation with Mach number of Reynolds number, based on mean aerodynamic chord, and wing-tip helix angle.

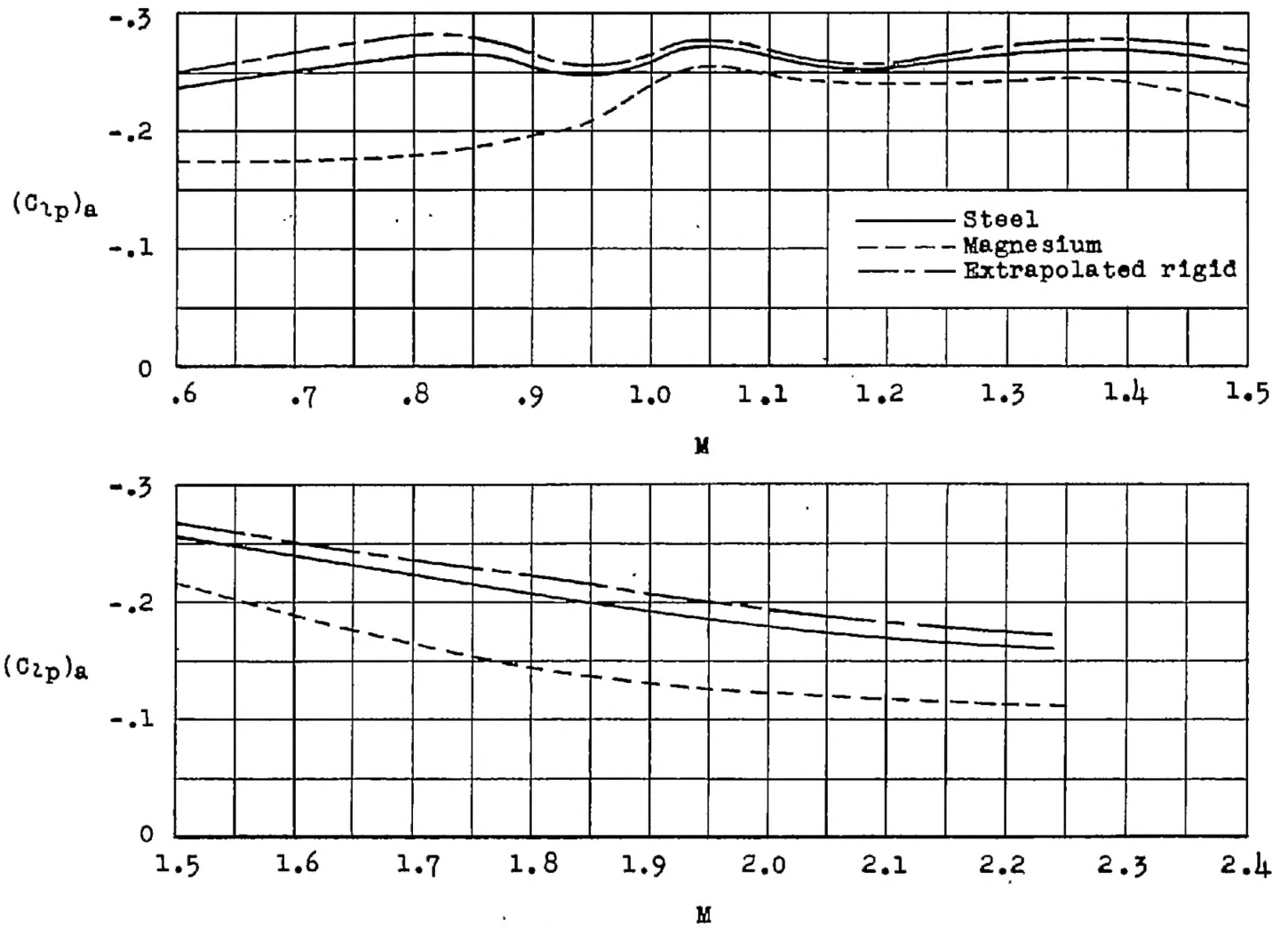

Figure 8.- Variation with Mach number of damping-in-roll derivative with adjustment for wing misalinement.

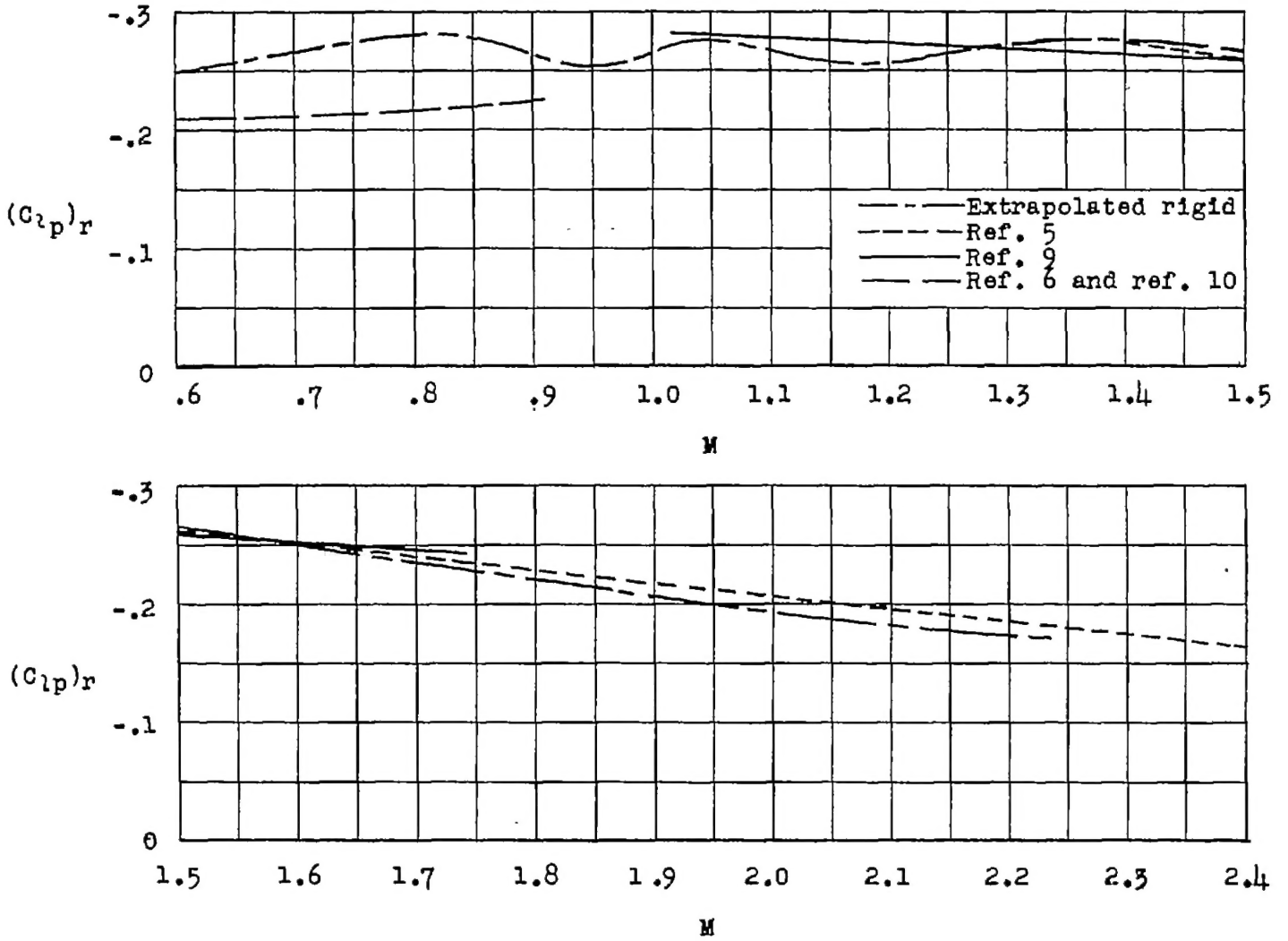

Figure 9.- Extrapolated rigid damping-in-roll derivative compared with values from other sources.